

Jahn-Teller orbital glass state in the expanded fcc Cs₃C₆₀ fulleride

Supplementary information

Anton Potočnik¹, Alexey Y. Ganin², Yasuhiro Takabayashi³, Martin T. McDonald³, Ivo Heinmaa⁴, Peter Jeglič^{1,5}, Raivo Stern⁴, Matthew J. Rosseinsky^{2,*}, Kosmas Prassides^{3,6*}, and Denis Arčon^{1,7,*}

¹ Jožef Stefan Institute, Jamova cesta 39, 1000 Ljubljana, Slovenia

² Department of Chemistry, University of Liverpool, Liverpool L69 7ZD, UK

³ Department of Chemistry, Durham University, Durham DH1 3LE, UK

⁴ National Institute of Chemical Physics and Biophysics, Akadeemia tee 23, 12618 Tallinn, Estonia

⁵ EN-FIST Centre of Excellence, Dunajska cesta 156, 1000 Ljubljana, Slovenia

⁶ WPI Research Center, Advanced Institute for Materials Research, Tohoku University, Sendai 980-8577, Japan

⁷ Faculty of mathematics and physics, University of Ljubljana, Jadranska cesta 19, 1000 Ljubljana, Slovenia

High-temperature static ¹³³Cs NMR spectra of fcc Cs₃C₆₀

The measured ¹³³Cs NMR spectrum arises entirely from the fcc Cs₃C₆₀ polymorph, as the weak resonances of the minority A15 Cs₃C₆₀ and bcc Cs₄C₆₀ phases are further suppressed by the appropriate choice of pulse sequences and pulse lengths,¹ while that of CsC₆₀ is very weak and shifted outside the spectral region to ~900 ppm.² In fcc A₃C₆₀ fullerides, two alkali ions per C₆₀ occupy the tetrahedral (T) and one alkali ion per C₆₀ the octahedral (O) sites.³ This leads to an expected intensity ratio of 2:1 for the two peaks, T and O in static alkali-metal NMR spectra, as indeed observed for Rb₃C₆₀ at high temperatures (>440 K).⁴ However, on cooling, the peak associated with the tetrahedrally coordinated ions splits into two components (labeled T and T'). The clear correlation between the temperature at which the C₆₀³⁻ units start to rotate on the NMR time-scale and the temperature at which the doublet T and T' structure collapses into a single resonance in static NMR experiments the unexpected splitting has been associated with the freezing in of the merohedral disorder.⁴⁻⁸ Namely, as the C₆₀³⁻ dynamics

slow down on the NMR time-scale, the intensity of the T' peak grows until it saturates at ~19% of the total tetrahedral-site NMR intensity. For instance, in the case of Rb_3C_{60} , the T' peak appears at around 380 K and its intensity saturates below 300 K.⁶ In the case of K_3C_{60} with an even smaller unit cell, the same process takes place between 230 and 200 K.⁴ In this respect, the observation of T-T' and O-O' splitting with the already saturated relative intensity of the T' peak at ~19% in the static ^{133}Cs NMR spectra measured on the fcc Cs_3C_{60} powder at 380 K (Fig. S1) unambiguously demonstrates that the C_{60}^{3-} anions are already completely static on the NMR time-scale. Moreover, the temperature independent relative intensities of the T' and O' peaks for all temperatures below 380 K mean that the merohedral disorder is frozen in for $T \leq 380$ K, i.e. at all temperatures relevant in this study.

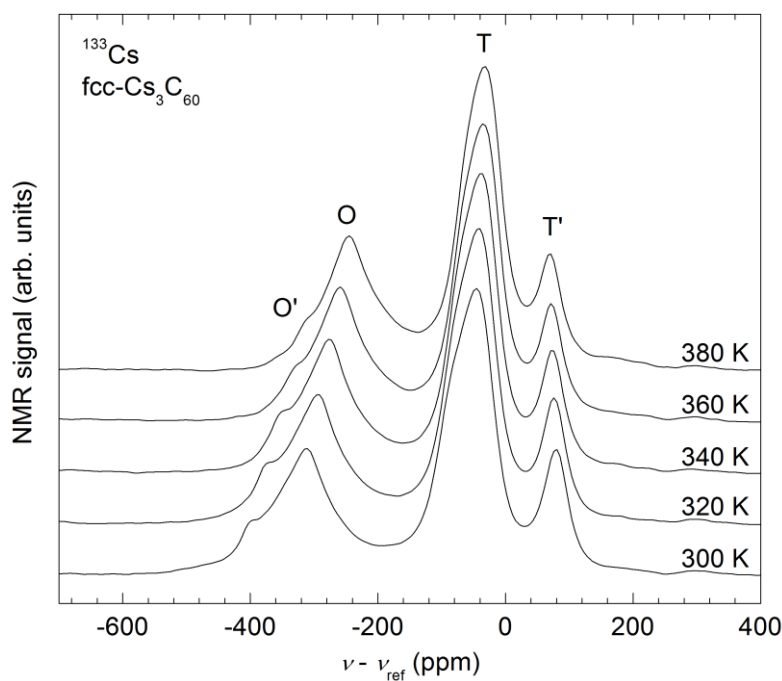


Figure S1: Static ^{133}Cs NMR spectra measured on the fcc Cs_3C_{60} powder between room temperature and 380 K clearly show that the T-T' and O-O' splitting is robust thus proving that the rotational dynamics of C_{60}^{3-} anions are completely frozen for all $T \leq 380$ K.

The analysis of ^{133}Cs and ^{13}C MAS NMR spectra of fcc Cs_3C_{60}

Room temperature ^{133}Cs MAS NMR spectrum. Seven peaks can be directly resolved in the measured room-temperature ^{133}Cs MAS NMR spectrum (Fig. 2a, main text) of Cs_3C_{60} . The differing coordination environment of the Cs^+ ions in the octahedral and tetrahedral interstices of the fcc unit cell (Fig. 2b-i, main text) is clearly reflected in the grouping of the ^{133}Cs NMR peaks in two distinct spectral regions. The difference in alkali-metal local coordination is also evident in the other spectral parameters (Table S1). Different peaks can be grouped on the basis of their spin-lattice relaxation times, T_1 : all

components of the tetrahedral site manifold exhibit short T_1 s (53-79 ms), while the T_1 s of the octahedral peaks are in the range of 230-380 ms. Similarly, the peak widths of the tetrahedral peaks (18-21 ppm) are consistently larger than those of the octahedral peaks (11-15 ppm). These spectral characteristics provide additional definitive support for the peak assignment of the observed resonances.

Table S1: Extracted parameters of the ^{133}Cs and ^{13}C MAS NMR resonances of fcc Cs_3C_{60} at room temperature.

^{133}Cs peaks	O'	O**	O	O*	T*	T	T'
Center (ppm)	-384.8(2)	-326.2(1)	-295.3(1)	-272.1(1)	-63.2(1)	-24.6(1)	94.8(1)
Width (ppm)	10.9(4)	13.4(2)	10.9(2)	14.8(3)	21.2(2)	20.1(1)	17.7(2)
Intensity (%)	1.4(1)	6.1(1)	11.3(2)	5.8(1)	24.8(2)	36.3(2)	14.2(1)
T_1 (ms)	230(10)	340(10)	370(10)	380(10)	79(3)	72(3)	53(3)
^{13}C peaks	C2	C3	C1				
Center (ppm)	212.1(5)	200.7(5)	183.7(5)				
Width (ppm)	7.1(4)	9.0(8)	6.5(3)				
Intensity (%)	40	40	20				
T_1 (ms)	51(3)	52(3)	80(10)				

Table S2: ^{133}Cs NMR O-site intensities in merohedrally disordered fcc Cs_3C_{60} . The configuration label, klm (first column) specifies the number of 6:6 C_{60} fusions around each O site directed along the x -, y -, or z -direction, respectively. The corresponding numbers of occurrences of each configuration are in the second column. The relative magnitude of the O-site local magnetic field (B_{loc} , third column) for each configuration is calculated as the vector sum of the six contributions from the 6:6 contact bonds of the neighboring C_{60}^{3-} ions. The assignment of the observed four components in the ^{133}Cs MAS NMR spectrum (Fig. 2) is in the fourth column. The total magnetic field at each distinct O site, B_{loc} can be then determined as the vector sum of the individual magnetic field contributions of the six neighboring C_{60}^{3-} units, assuming that the direction of each contribution is defined by the orientation of the relevant contact 6:6 bond. The calculated relative magnitudes of B_{loc} at each distinct O site for the different klm configurations ($\sqrt{12}$, $\sqrt{14}$, $\sqrt{18}$, and $\sqrt{20}$) are in good qualitative agreement with the observed shifts of the four components of the O-site ^{133}Cs NMR spectrum ($-272.1(1)$, $-295.3(1)$, $-326.2(1)$, and $-384.8(2)$ ppm; Fig. 2a, Table S1).

klm	No. of possibilities	B_{loc} , relative magnitude	O-peak label
222	10	$\sqrt{12}$	O*
321	36	$\sqrt{14}$	O
411 & 330	12	$\sqrt{18}$	O**
420	6	$\sqrt{20}$	O'

Analysis of the temperature dependence of ^{133}Cs MAS NMR peaks. On cooling all ^{133}Cs MAS NMR peaks strongly shift and broaden (Fig. 3, main text) due to the additional disorder in the octahedral and tetrahedral local-site configurations associated with the freezing out of Jahn-Teller dynamics of the C_{60}^{3-} anions. This makes the analysis of the low-temperature ^{133}Cs MAS NMR spectra less straightforward. In order to follow the spectral changes with decreasing temperature, we fitted the measured spectra with seven overlapping Gaussian peaks whose relative intensities were kept fixed according to Table S1 for temperatures between 300 and 103 K. Between 103 and 60 K, the T* and O* peaks become indistinguishable from the main T and O peaks, respectively. Therefore, when fitting the ^{133}Cs MAS NMR spectra between 89 and 60 K, their intensities were included into those of T and O peaks. Following this fitting strategy, we succeeded in simulating all spectra consistently between 300

and 60 K (Fig. S2). A similar approach could be also applied in the analysis of the spectrum collected at 51 K. However, due to the considerable overlap between the T' and T peaks at this temperature, the linewidth of the T' peak is subject to a large error. The temperature dependence of the derived peak shifts is shown in Fig. 3b of the main text. The temperature dependence of the peak widths is shown in Fig. S3a.

Analysis of the temperature dependence of ^{13}C MAS NMR peaks. A similar fitting strategy can be also applied to analyse the ^{13}C MAS NMR spectra (Fig. 1a, main text). However, because of significant overlap between the peaks, it is very difficult to extract individual widths for the C1-C3 peaks below 195 K. Therefore, in order to follow consistently the linewidth of the ^{13}C MAS NMR spectra, we here focus on the full width at half maximum (inset to Fig. S3b). It is clear that the ^{133}Cs (Fig. S3a) and ^{13}C (Fig. S3b) MAS NMR peak linewidths show qualitatively very similar temperature dependences. This suggests that the additional contributions to the MAS NMR linewidth, which cannot be averaged out by rapid spinning, originate from the additional distribution of individual resonances induced by the local-site symmetry breaking mechanism.

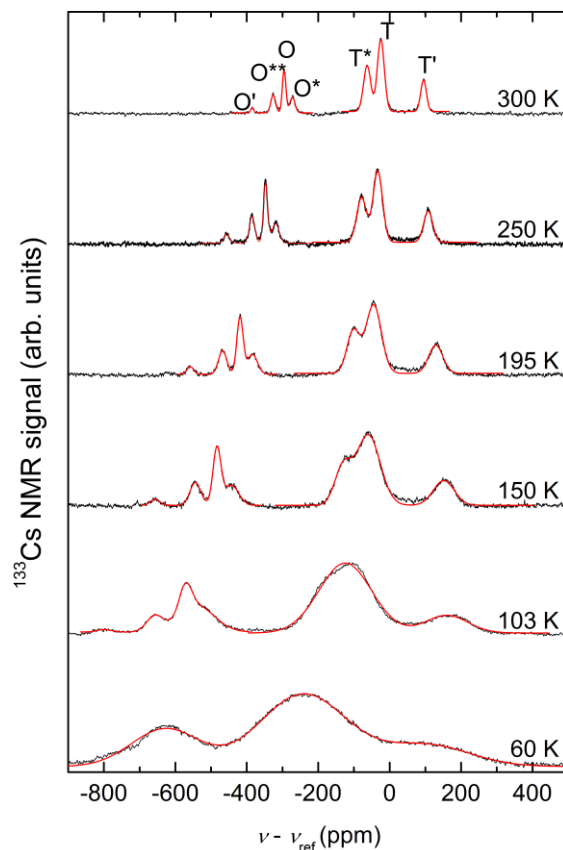


Figure S2: High-resolution ^{133}Cs MAS NMR spectra of fcc Cs_3C_{60} at different temperatures (black solid lines) and their fits with multi-Gaussian-component models (red solid lines). In all cases, the spinning frequency was $\nu_R = 25$ kHz.

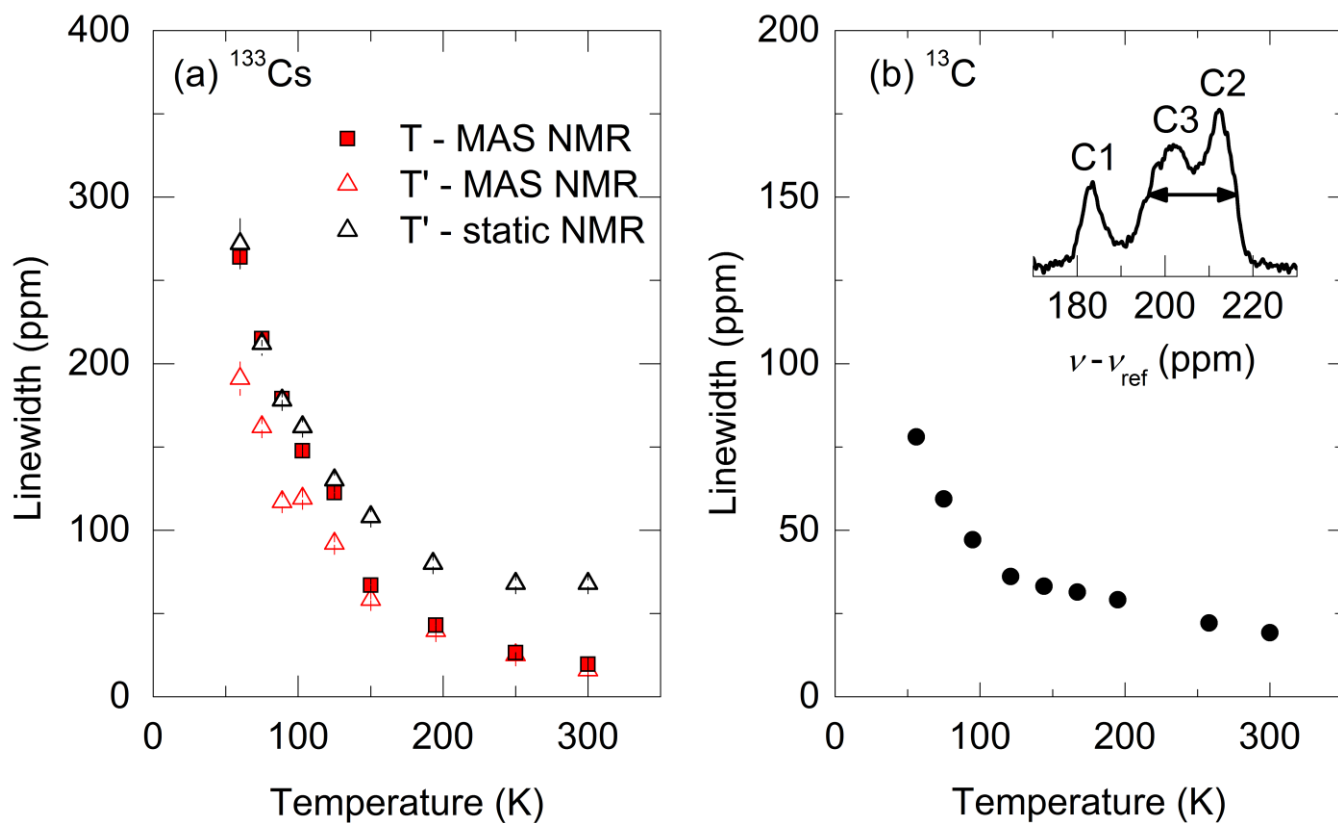


Figure S3: (a) Temperature dependence of the T (red solid squares) and T' (red open triangles) ^{133}Cs NMR linewidths as determined from the fitting of the high-resolution ^{133}Cs MAS NMR spectra of fcc Cs_3C_{60} (Fig. S2). The temperature evolution of the T' (black open triangles) static ^{133}Cs NMR linewidth is also shown for comparison. (b) Temperature dependence of the full width at half maximum of the ^{13}C MAS NMR spectra. *Inset:* Room temperature ^{13}C MAS NMR spectrum with the definition of the full width at half maximum marked by arrow.

Determination of ^{133}Cs hyperfine coupling constants. ^{133}Cs MAS NMR peak positions depend on the chemical shift and the hyperfine interactions with the neighboring C_{60}^{3-} moments. The latter directly probe the spin susceptibility, which is expected to follow the Curie-Weiss law, $\chi = C/(T - \theta)$ in the insulating state where C and θ are the Curie constant and the Curie-Weiss temperature, respectively. We thus proceeded by expressing the temperature-dependent shift as:

$$^{133}\nu_i = ^{133}\nu_{\text{CS},i} + \frac{^{133}a_i}{N_A\mu_B}\chi, \quad (1)$$

where $^{133}\nu_{\text{CS},i}$ and $^{133}a_i$ are the corresponding chemical shifts and hyperfine coupling constants, respectively for each ^{133}Cs peak i . N_A is the Avogadro number, μ_B the Bohr magneton, and χ is the bulk spin susceptibility. Model (1) fits the corresponding shifts of all ^{133}Cs T-peaks ($i = 1-7$) in the temperature range 125 to 300 K and O-peaks in the temperature range 60 to 300 K if the same $\theta = -240(30)$ K is taken as a global Curie-Weiss temperature.

Next task is to extract the corresponding hyperfine coupling constants. A standard method is to plot the shifts against the bulk spin susceptibility, χ with temperature as an implicit parameter – the so-called Clogston-Jaccarino plot⁹ (Fig. S4). For temperatures higher than 125 K, a perfect linear scaling with the measured χ (¹) is observed for all peaks and we can thus reliably extract both $^{133}a_i$ and $^{133}\nu_{\text{CS},i}$ parameters for each ^{133}Cs resonance (Table S3). The $^{133}\nu_{\text{CS},i}$ shifts typically fall into the range expected for the Cs^+ ions. However, we notice that the values of $^{133}a_i$ strongly depend on the Cs^+ coordination: the $^{133}a_i$ values for the octahedral peaks lie between -1.9 and -3.2 kOe/ μ_B , whereas those for the tetrahedral peaks are much smaller in magnitude and can even change sign, as is the case for the T' peak. The departure from linear scaling behavior in the Clogston-Jaccarino plot for the T-sites below 125 K is consistent with their high sensitivity towards the JT-dynamics of the C_{60}^{3-} units where the merohedral disorder plays a decisive role in tuning the crystal field.

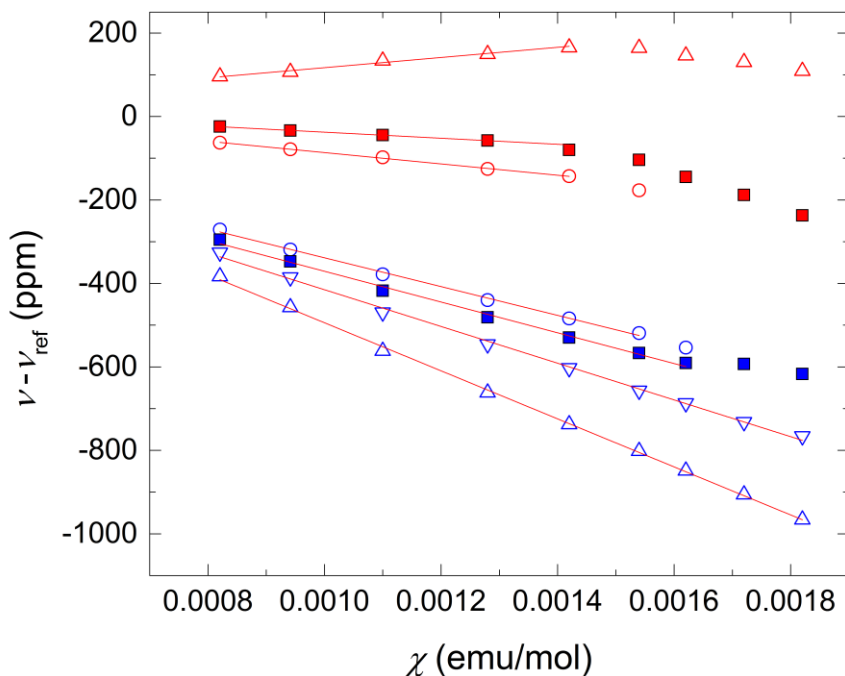


Figure S4: Clogston-Jaccarino plot of the ^{133}Cs MAS NMR shifts plotted against the bulk spin susceptibility, χ for the Cs_3C_{60} powder.¹ Fits (solid lines) yield hyperfine coupling constants, $^{133}a_i$ for all seven peaks summarized in Table S2 (see text for details).

Table S3: The hyperfine coupling constants, $^{133}a_i$, and the chemical shifts, $^{133}v_{CS,i}$, for the ^{133}Cs NMR peaks in Cs_3C_{60} powder, as extracted from the Clogston-Jaccarino plot (Fig. S4).

	O'	O**	O	O*	T*	T	T'
$^{133}a_i$ [kOe/ μB]	-3.2(1)	-2.5(1)	-2.6(1)	-1.9(1)	-0.8(1)	-0.4(1)	0.7(1)
$^{133}v_{CS,i}$ [ppm]	81(8)	25(10)	2(14)	6(11)	49(6)	35(2)	-5(13)

References

1. A. Y. Ganin, Y. Takabayashi, P. Jeglič, D. Arčon, A. Potočnik, P. J. Baker, Y. Ohishi, M. T. McDonald, M. D. Tzirakis, A. McLennan, G. R. Darling, M. Takata, M. J. Rosseinsky, and K. Prassides, *Nature*, 2010, **466**, 221–225.
2. V. Brouet, H. Alloul, F. Quéré, G. Baumgartner, and L. Forró, *Phys. Rev. Lett.*, 1999, **82**, 2131–2134.
3. P. W. Stephens, L. Mihaly, P. L. Lee, R. L. Whetten, S.-M. Huang, R. Kaner, F. Deiderich, and K. Holczer, *Nature*, 1991, **351**, 632–634.
4. R. E. Walstedt, D. W. Murphy, and M. Rosseinsky, *Nature*, 1993, **362**, 611–613.
5. H. Alloul, K. Holczer, Y. Yoshinari, and O. Klein, *Phys. C Supercond.*, 1994, **235–240**, 2509–2510.
6. Y. Yoshinari, H. Alloul, V. Brouet, G. Kriza, K. Holczer, and L. Forro, *Phys. Rev. B*, 1996, **54**, 6155.
7. M. Kraus, O. Klein, G. Buntkowsky, and K. Lüders, *Phys. B Condens. Matter*, 1999, **271**, 7–14.
8. Y. Yoshinari, H. Alloul, K. Holczer, and L. Forro, *Phys. C Supercond.*, 1994, **235–240**, 2479–2480.
9. A. M. Clogston and V. Jaccarino, *Phys. Rev.*, 1961, **121**, 1357–1362.